Simulations of Primary and Secondary Gas Penetration for a Gas-Assisted Injection-Molded Thin Part with Gas Channel

SHIA CHUNG CHEN, NIEN-TIEN CHENG, SHENG-YAN HU

Mechanical Engineering Department, Chung Yuan University, Chung-Li, Taiwan 32023, Republic of China

Received 4 June 1997; accepted 9 June 1997

ABSTRACT: Numerical simulations and experimental studies concerning melt flow and primary as well as secondary gas penetration during the filling and the postfilling stages in gas-assisted injection molding of a thin plate with a semicircular gas channel design were conducted. Distribution of the skin melt thickness along the gas-penetration direction was measured to identify primary and secondary gas penetration. Melt and gas flow within the gas channel of a semicircular cross section is approximated by a model which uses a circular pipe of an equivalent hydraulic diameter superimposed on the thin part. An algorithm based on the control-volume/finite-element method combined with a dual-filling parameter technique suitable for the tracing of two-component flow-front advancements is utilized and numerically implemented to predict both melt- and gas-front advancements during the melt-filling and the gas-assisted filling processes. A flow model of the isotropic melt-shrinkage origin combined with a gapwise layer tracing algorithm was implemented to assist the prediction of secondary gas penetration and melt flow in the post-filling stage. Simulated results on the gas front locations at the end of both primary and secondary penetration phases show reasonably good coincidence with experimental observations. © 1998 John Wiley & Sons, Inc. J Appl Polym Sci **67:** 1553–1564, 1998

Key words: gas-assisted injection molding; primary and secondary gas penetration; gas channel

INTRODUCTION

Gas-assisted injection molding (GAIM) is one of the innovative multicomponent injection-molding processes recently developed. In gas-assisted injection molding, the mold cavity is partially filled with the polymer melt followed by the injection of inert gas into the core of the polymer melt.[1–4] A schematic diagram of gas-assisted injection molding is illustrated in Figure 1. During the filling phase, the gas cores out the hot melt at the gap center and penetrates into the cavity. Gas penetration in the filling phase is designated as the primary gas penetration. In the postfilling stage, gas continues to penetrate as a result of melt shrinkage. This period is identified as the secondary gas penetration. A schematic is shown in Figure 2. Compared with conventional injection molding, the required injection pressure is greatly reduced. As a result, residual stress and warpage within the molded part can be minimized and the part quality can be improved. Despite the advantages associated with the process, the molding window and process control become more critical and difficult since additional processing parameters are involved. These new gas-related processing parameters include the amount of melt injection, gas pressure, delay time of gas injection, and gas injection time. During the gas-injection stage, gas usually takes the path of the least resis-

Correspondence to: S. C. Chen.

Contract grant sponsor: National Science Council (China); contract grant number: 84-2622-E033-002R.

Journal of Applied Polymer Science, Vol. 67, 1553–1564 (1998)

 CCC 0021-8995/98/091553-12

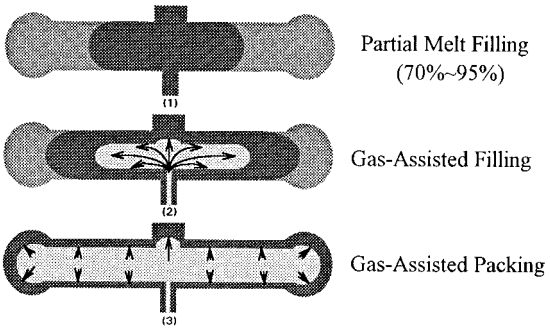

Figure 1 Schematic of gas-assisted injection-molding process.

tance to catch up with melt front. To guide the gas flow to the desired location and/or the designed distribution, the part design using thick ribs as gas channels also becomes a dominant factor for the successful application of the process. In general, due to the complexity of the gas-channel design, the process control as well as different flow characteristics between the gas and melt, computer simulation is expected to become an important and a required tool to help with both part design and process evaluation in the coming age.

For nearly a decade, a simulation model based on the Hele–Shaw type of flow has been being developed to describe the polymer melt flow in thin cavities during conventional injection moldings. Two typical types of control volume/finite element formulations were employed.[5,6] These simulations provide acceptable predictions from the engineering application point of view. Now, the existing models meet a new challenge and must be adopted to handle both gas and melt flows in cavities of nonuniform thickness. Although a complete three-dimensional analysis may be the final solution, the computational cost is too expensive to be implemented at the present stage for engineering-design purposes. At the present stage, a numerical algorithm suitable for the simulation of both gas- and melt-front advancements as well as an empirical model describing the cored out melt thickness between the solidified melt and gas/melt interface (Fig. 2) in the filling process as a function of processing parameters, material properties and/or flow geometry are both required for an accurate simulation of the gas-assisted injection-molding process. For parts laid out with gas channels, which are usually of a pipelike flow leader, a flow algorithm should also be adjusted to describe these mixed 1-D and 2-D flow characteristics. The most popular approach for dealing with melt flow and gas penetration is to utilize a circular pipe of an equivalent hydraulic diameter and a superimposition approach[7] to represent the mixed 1-D and 2-D flow characteristics for the melt and gas flow in the gas channel of a noncircular cross section. Such an analysis verified for melt flow in a thin cavity with a rib of semicircular cross section was reported recently.[7] An algorithm based on the control-volume/finite-element method combined with a particle-tracing scheme using a dual-filling parameter technique was developed to simulate both gas and polymer melt flow during the filling process of gas-assisted injection molding. This particle-tracing scheme is modified from the algorithm concept successfully used for the calculation of skin and core melt-front advancements during the coinjection-molding process.[8] Although studies on the numerical simulations are in progress,[3,9,10] attention has been focused on the gas- and melt-front advancements during the filling stage. Significant gas penetration may occur during the post-filling stage as a result of melt shrinkage. Characteristics of gas penetration in the primary phase and secondary phase are quite different, resulting in a different distribution profile in the skin melt thickness formation.[11] Simulations of secondary gas penetration based on a pressure-induced flow model used in commercial packages such as C-GASFLOW and Moldflow/gas show underpredicted results.[12] To avoid the calculation of gapwise velocity which would require 3-D computation, an isotropic-shrinkage-induced flow model was developed to predict secondary gas penetration. The present numerical algorithms and the associated simulations were first applied to a gas injection-molded spiral tube of purely 1-D flow. Comparison of the predicted results with experiments shows positive confirmation. Then, a thin-plate part laid out with a gas channel of a semicircular cross section was gas-assisted injection-molded. The skin melt thickness between

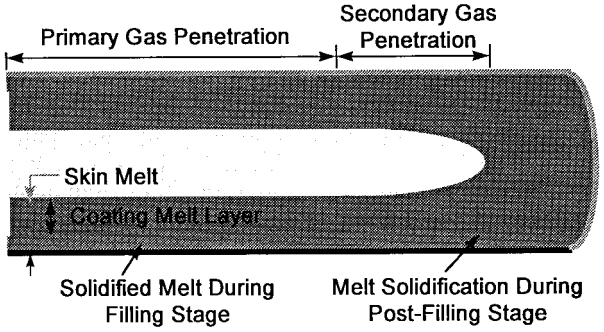

Figure 2 Schematic of primary and secondary gas penetrations in GAIM process.

the solidified melt and gas was investigated and measured along the gas-flow direction. Simulated results for the advancements of the melt and gas front within the filling period as well as the secondary gas penetration in the postfilling phase are illustrated and discussed. The predicted distribution of gas penetration is compared with experimental observation.

MODELING AND FORMULATION

It has been generally accepted that a Hele–Shaw type of flow model provides a reasonably accurate description of polymer melt flow in a 3-D thin cavity. As a result, the relevant governing equations for the inelastic, non-Newtonian fluid flow under nonisothermal conditions are similar to those used in conventional injection molding[5,6,13]:

$$0 = \frac{\partial}{\partial z}\left(\eta \frac{\partial u}{\partial z}\right) - \frac{\partial P}{\partial x} \tag{1}$$

$$0 = \frac{\partial}{\partial z}\left(\eta \frac{\partial v}{\partial z}\right) - \frac{\partial P}{\partial y} \tag{2}$$

$$\frac{\partial \rho}{\partial t} + \frac{\partial}{\partial x}(b\bar{u}) + \frac{\partial}{\partial y}(b\bar{v}) = 0 \tag{3}$$

$$\rho C_P\left(\frac{\partial T}{\partial t} + u\frac{\partial T}{\partial x} + v\frac{\partial T}{\partial y}\right) = \frac{\partial}{\partial z}\left(k\frac{\partial T}{\partial z}\right) + \eta\dot{\gamma}^2 \tag{4}$$

where P, T, u, and v represent pressure, temperature, and melt velocities in the x and y directions, respectively. b is the half-thickness of the mold cavity in the gapwise direction, z. $\bar{u}$ and $\bar{v}$ are averaged velocities gapwisely for u and v, correspondingly. In addition, $\dot{\gamma}$, η, ρ, C_p, and k are the shear rate, viscosity, density, specific heat, and thermal conductivity for the polymer melt, respectively.

Non-Newtonian characteristics of the polymer melt viscosity is described by a form of a modified-Cross model with Arrhenius temperature dependence, i.e.:

$$\eta(T, \dot{\gamma}) = \frac{\eta_0(T)}{1 + (\eta_0\dot{\gamma}/\tau^*)^{1-n}} \tag{5}$$

with

$$\eta_0(T) = B\,\mathrm{Exp}\left(\frac{T_b}{T}\right)\mathrm{Exp}(\alpha P) \tag{6}$$

During the postfilling stage, gas continues to penetrate as a result of melt shrinkage. Calculation of the melt shrinkage and compressibility of the polymer melt is based on the P–V–T equation of state by Tait in the form of

$$\nu(P, T) = \nu_0(T)\{1 - C\ln[1 + P/B(T)]\} + \nu_t(T, P) \tag{7}$$

where

$$\nu_0(T) = \beta_1 + \beta_2(T - \beta_5)$$
$$B(T) = \beta_3 \cdot \mathrm{Exp}[-\beta_4 \cdot (T - \beta_5)]$$
$$T_t(P) = \beta_5 + \beta_6 \cdot P$$
$$\nu_t(P, T) = \beta_7 \cdot \mathrm{Exp}[\beta_8(T - \beta_5) - \beta_9 \cdot P]$$

β_1, β_2, β_3, β_4, β_5, β_6, β_7, β_8, and β_9 are material constants.

Equations (1) and (2) can be integrated into eq. (3) in the form of

$$G(P, T)\frac{\partial P}{\partial t} + \frac{\partial}{\partial x}\left(-S\frac{\partial P}{\partial x}\right) + \frac{\partial}{\partial y}\left(-S\frac{\partial P}{\partial y}\right) = F(P, T) \tag{8}$$

with

$$S = \int_0^b \frac{z^2}{\eta}\,dz \tag{9}$$

$$G(P, T) = \int_0^b \left\{\frac{C}{[B(T) + P]\{1 - C\ln[1 + P/B(T)]\}}\right\} dz \tag{10}$$

$$F(P, T) = \int_0^b \left\{\frac{\beta_2}{\nu_0(T)} - \frac{C \cdot P \cdot \beta_4}{\{1 - C\ln[P/B(T)][B(T) + P]\}}\right\}\frac{\partial T}{\partial t}dz \tag{11}$$

If in the melt-filling and gas-assisted filling stages the compressibility of the polymer melt is neglected, eq. (8) can be reduced to

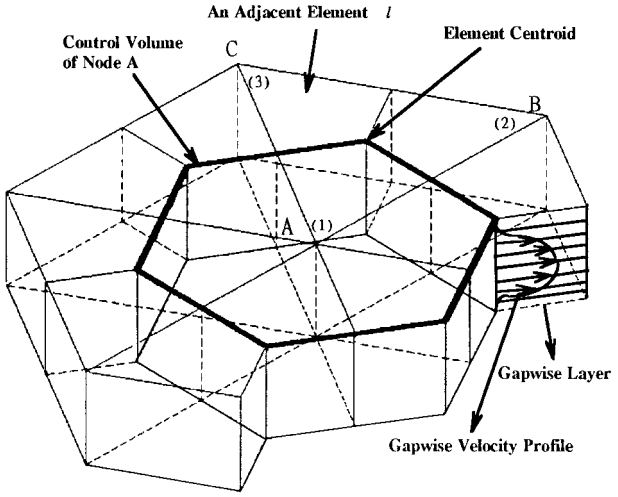

Figure 3 Schematic of a control volume centered at node A. Control volume is constructed by connections of the centriods of all the adjacent finite elements around node A.

$$\frac{\partial}{\partial x}\left(S\frac{\partial P}{\partial x}\right)+\frac{\partial}{\partial y}\left(S\frac{\partial P}{\partial y}\right)=0 \qquad (12)$$

NUMERICAL ALGORITHM

Algorithm for Melt-front Advancement During Melt Injection

Melt Flow in Conventionally Injection-molded Thin Cavities

In solving for the pressure field during the melt-injection period, eq. (12) of the Laplacian form is discretized using a standard Galerkin finite element method.[14] The control volume formulation can also be employed directly to obtain the same discretized form.[5,6,13] The net flow, $q_i^{(\ell)}$, that enters its control volume, centered at node A (Fig. 3), from an adjacent element ℓ, can be represented by

$$q_i^{(\ell)}=S^{(\ell)}\cdot\sum_{k=1}^{2\text{ or }3}\cdot D_{ik}^{(\ell)}\cdot P_k^{(\ell)} \qquad (13)$$

where i is the local index for node A in element ℓ and i = 1, 2, or 3 for triangular elements and i = 1 or 2 for rodlike elements. Subscript k denotes the local node index in element ℓ and $D_{ik}^{(\ell)}$ is the influence coefficient of the nodal pressure to the net flow in element ℓ. Linear interpolation functions are used for both types of elements. Values of $D_{ik}^{(\ell)}$ are equal to

$$D_{ik}^{(\ell)}=\sum_{k=1}^{3}\frac{B_iB_k+C_iC_k}{4_\Delta^{(\ell)}} \qquad (14)$$

and

$$D_{ik}^{(\ell)}=(-1)^{i+k}\frac{\pi}{2_L^{(\ell)}} \qquad (15)$$

for a triangular element and a rodlike element, respectively. $\Delta^{(\ell)}$ is the area of the triangular element ℓ, and $L^{(\ell)}$ is the length of the rod element. $B_1=y_2-y_3$ and $C_1=x_3-x_2$, where x and y are planar coordinates of the nodes in the triangular element. The other coefficients are obtained by cyclically permuting the subscripts. At the entrance, the net flows from all adjacent elements must satisfy the following relation:

$$\sum_\ell q_i^\ell=\frac{Q}{2} \qquad (16)$$

where Q is the total volumetric flow rate of the polymer melt. For the interior nodes, the net flows from all adjacent elements obey the conservation law of mass and are equal to zero, i.e.:

$$\sum_\ell q_i^\ell=0 \qquad (17)$$

Equations (16) and (17) can be finally integrated and described in a matrix form as

$$[K]\{P\}=\{G\} \qquad (18)$$

where $[K]$ is the element coefficient matrix; $\{P\}$ is the column matrix associated with pressure, P; and $\{G\}$ is the column matrix for the variable, G_m. $G_m=Q/2$, if m, represented in global node index number, is the entrance node of the polymer melt. Otherwise, $G_m=0$.

In solving eq. (18), the boundary conditions at the melt-front boundary, cavity side wall, and melt inlet region must also be specified. At the melt-front nodes, the nodal pressures are equal to zero (gauge pressure), i.e.:

$$P=0 \qquad (19)$$

Along the cavity side wall where the melt is impermeable, the boundary condition is specified as

$$\frac{\partial P}{\partial n} = 0 \tag{20}$$

Since in deriving eq. (18) for nodes located on the cavity side, the melt-flow rate across the cavity side wall is assumed to be zero; therefore, the boundary condition in the form of eq. (20) is automatically fulfilled. Near the melt entrance region, the boundary conditions are specified according to the operation conditions of the melt- and gas-injection system. If the pressure is prescribed, then

$$P|_{\text{entrance}} = P_{\text{injection}} \tag{21}$$

and $P_{\text{injection}}$ is the injection pressure at the entrance. If the volumetric flow rate is defined, then the boundary condition is expressed by

$$\oint_c \left(-S \frac{\partial P}{\partial n} \right) ds = \frac{Q}{2} \tag{22}$$

where C is any closed contour lying in the melt-filled region and the enclosing melt entrance. In the present article, the melt flow rate, Q, is determined from the filling speed during the melt-injection period, whereas gas pressure is defined during the gas-injection period. In the former case, eq. (22) is automatically satisfied when applying eq. (16). To verify the numerical convergence in every analysis step, mass conservation at the melt entrance expressed by eq. (17) is also checked once pressure and flow rate $q_i^{(\ell)}$ in each subelement are obtained. When gas pressure is prescribed during the gas-injection period, the flow rate at the materials entrance is treated as an unknown and a variable rearrangement in the matrix described by eq. (19) is required.

To distinguish the entrance node and the interior nodes from the melt-front nodes, a filling parameter f_{melt} is defined and calculated during all analyses. f_{melt} is equal to 1 for the entrance node and interior nodes, whereas $0 < f_{\text{melt}} < 1$ for the melt-front nodes. When f_{melt} is 0, the node is designated as an empty node. A schematic of the node definition is shown in Figure 4(a). At the melt-front nodes, the net flow entering the control volume from neighboring elements which are filled with melt can be computed. Then, the corresponding filling time required for filling the rest control volume of each melt-front node can be also obtained. The analysis interval is chosen as the minimum of these filling times. By doing so, only one melt-front node gets filled per step. Once the pressure field is solved, the gapwise velocity profile and the associated shear rate values can be calculated. At the melt fronts, a uniform profile for the temperature and gap-averaged velocity is assumed to account for the fountain flow effect. The numerical algorithm and procedure basically follow those reported.[5–7,13]

In solving for the temperature field, the same method reported previously is used.[5,13] The calculation of the nodal temperature is basically weighted from the subvolumes of all adjacent elements. However, the convection term and the viscous-heating term consider only the contribution of the upstream elements. An implicit method is used for the conduction term, whereas the convection and viscous-heating terms were evaluated at the earlier step. The iteration criteria and an algorithm are also similar to those used in conventional injection molding.[5,13]

Melt Flow in a Flow-leader-type Gas Channel of a Noncircular Cross Section

The geometry of the gas channel of a semicircular cross section together with the connection portion in the thin part is approximated by a circular pipe of an equivalent hydraulic diameter D_{eq}. D_{eq} can be computed according to the description in Figure 5 for a gas channel cross section of a semicircular shape. Also, the shape factor is defined and used to correct for the excess heat transfer caused by the extra area in using an equivalent diameter pipe. Once the shape factor value is obtained, it is combined with the thermal conductivity of the polymer melt to take the excess heat transfer into account. Then, the gas channel is modeled as a linear, two-node element which is superimposed on the part shell mesh of the triangular element. The situation is depicted in Figure 6. In the simulation, a true volumetric flow rate is obtained from the real part volume. In solving for the temperature field, the same method used for the regular, thin part is employed. However, the energy equation in cylindrical coordinates is used to solve for the temperature whenever the triangular part element node is superimposed on by the rodlike gas channel node. An experimental verification of the present approach was reported for melt-front advancement within a rib-type flow leader of a semicircular cross section during conventional injection molding.[7]

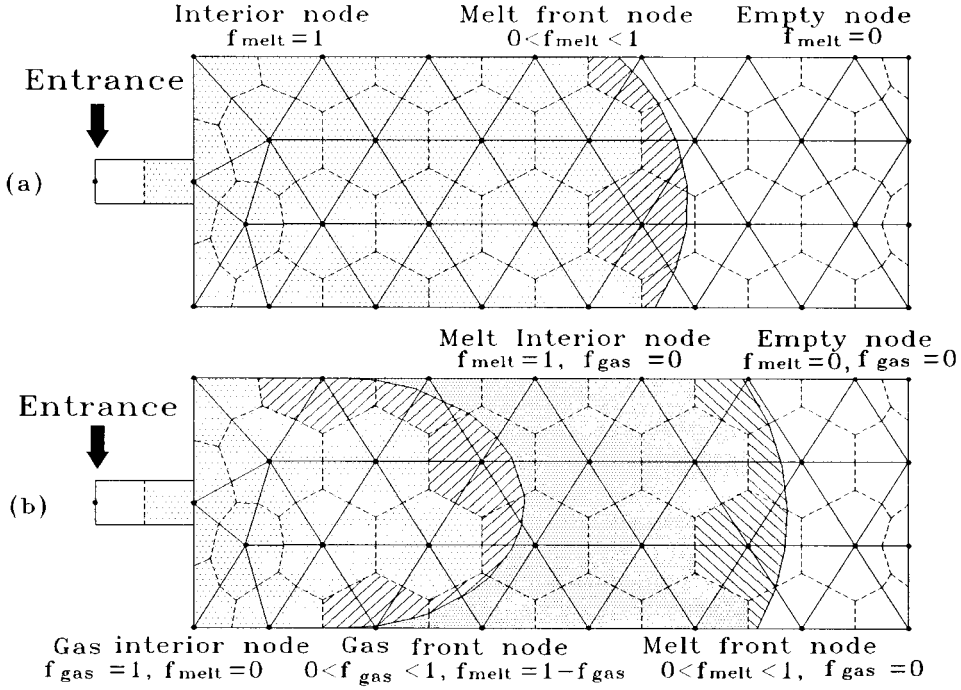

Figure 4 (a) Schematic of filling parameters used to identify the location of melt front during melt injection. (b) Filling parameters used to identify gas front nodes as well as gas interior nodes in gas-injection stage.

Algorithm for Gas- and Melt-front Advancements During the Filling Stage

Once the gas was injected into the mold either through a runner or cavity, the domain filled with gas is assumed to be of uniform pressure. The pressure at the gas-injection node is assumed to be at the injected gas pressure and the total flow rate of the melt is treated as an unknown. Once the melt-flow rate is solved, the gas-front advancement around the gas-injection node is determined by the melt-flow rate in each subelement of the control volume around this node. When the gas-front advances, it is necessary to introduce a secondary filling parameter, f_{gas}, to identify gas-front nodes and gas-interior nodes among the melt-interior nodes filled with melt at previous instants as specified in Figure 4(b). The algorithm is similar to our particle-tracing algorithm

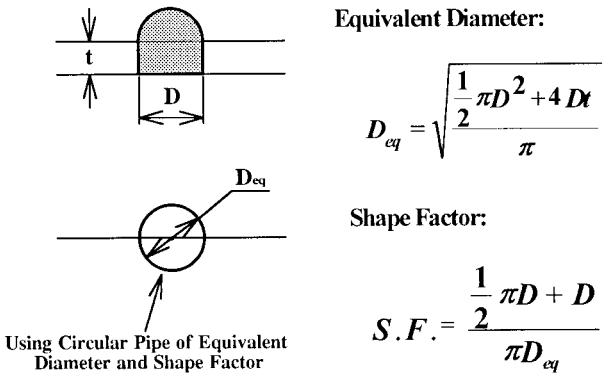

Figure 5 Circular pipe of equal cross-section area is used to represent the gas channel with a cross section of a semicircle and the connecting portion of the plate. Formulation of equivalent diameter as well as shape factor are also given.

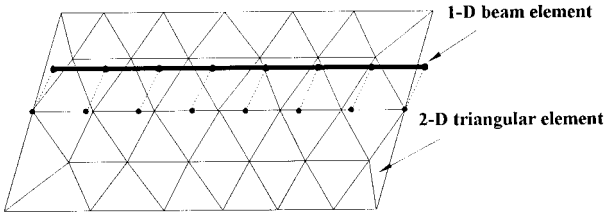

Figure 6 Schematic diagram for the superimposition of triangular shell element mesh and two-node beam element mesh representing the thin part and gas channel, respectively.

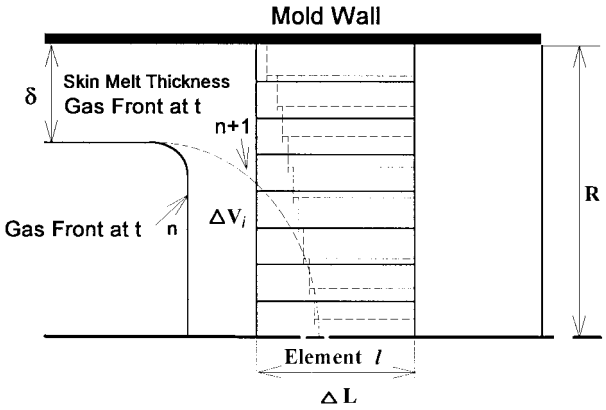

Figure 7 Schematic of the isotropic melt-shrinkage flow model used to assist the simulation of secondary gas penetration.

developed for both skin and core melt-front advancements in the coinjection-molding process reported recently.[8] Here, the injected gas was treated as a core material with an additional assumption that the pressure be uniform within the gas region. However, for gas-front nodes whose subelements contribute to the corresponding nodal control volume involve both melt-filled elements and gas-filled elements, a mass conservation law must be derived based on the available volume for gas filling by excluding that portion contributed by the coating melt. In solving for the temperature for the coating melt, a transient heat-conduction equation discretized by the finite difference method is used. The convection term and the viscous-heating term in the energy equation can be neglected. A convective boundary is assumed at the gas/melt interface using 30 W/m^2°C for the heat transfer coefficient of the gas. Due to the small time interval of the gas injection, heat transfer from the coating melt to the gas is negligible.

Algorithm for Secondary Gas Penetration During the Postfilling Stage

To solve for the pressure and temperature field during this period, the mathematical model and numerical scheme[15] used for the postfilling simulation in the conventional injection molding was implemented. The gas-filled domain is assumed to be of uniform pressure. Gas is assumed to penetrate toward the melt-filled-only region. However, when gapwisely averaged velocity or gapwisely profiled planar velocities combined with the layer control volume method were used to predict secondary gas penetration, neither gas-penetration length nor the geometry of the hollowed core caused by secondary gas penetration were consistent with experimental observations. This indicates that the pressure-induced melt-flow model for 2-D characteristics in a fluid flow used by the simulation of the postfilling process in the conventional injection molding cannot describe the melt-flow and secondary gas-penetration behavior. An isotropic melt-shrinkage model, which allows melt shrinkage along both the planar and the gaspwise directions, is assumed and implemented. To trace the gas-front advancement, the gas-filling parameter, f_{gas}, is now extended to each gapwise layer on the same control-volume/finite-element basis. A schematic is depicted in Figure 7. During each analysis step, the available volume in each gapwise layer resulting from melt shrinkage is calculated from the pressure and the temperature values using the P–V–T relationship described by eq. (7). Along the gapwise direction and the axial direction of the equivalent gas channel, 10 gapwise layers were used. The analysis continues until the gas is released and the part is rejected.

EXPERIMENTAL

A 75 ton Battenfeld 750/750 coinjection-molding machine and airmold system were used for the present experiments. The melt temperature for the PS resin is 230°C and the mold temperature was 40°C. A spiral tube part of 6 mm diameter and a uniform thin plate 3 mm thick designed with a gas channel of a semicircular section were gas injection-molded to provide experimental ver-

Table I Material Constants of P–V–T Equation for PS

	Liquid	Solid
β_1 (m^3/kg)	9.7805E − 4	9.7787E − 4
β_2 (m^3/kgK)	5.3356E − 7	2.8265E − 7
β_3 (Pa)	1.5688E + 8	1.9332E + 8
β_4 (K^{-1})	3.8794E − 3	6.3231E − 3
β_5 (K)	362.97	362.97
β_6 (K/Pa)	2.5021E − 7	2.5021E − 7
β_7 (m^3/kg)	1.8039E − 7	1.8039E − 7
β_8 (K^{-1})	0.097142	0.097142
β_9 (Pa^{-1})	4.387E − 9	4.387E − 9

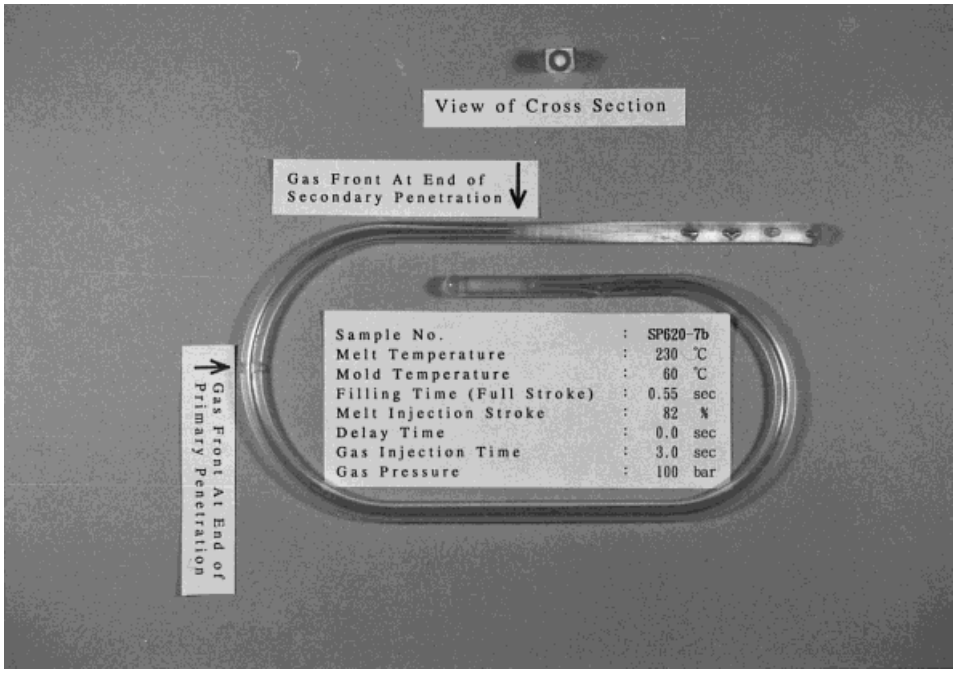

Figure 8 A gas-assisted injection-molded spiral tube.

ification for the present simulation scheme. In all cases, the skin melt thickness along the gas-flow direction was measured. Detailed experimental procedures were described elsewhere.[12]

For polystyrene (CHI MEI/PG33), materials constants in the modified-Cross model used for viscosity values are $n = 0.2838$, $\tau^* = 1.791E + 04$ Pa, $B = 2.591E - 07$ Pa-s, and $T_b = 11{,}680$ K. The density, specific heat, and thermal conductivity of PS are 940 kg/m^3, 2100 J/kg K, and 0.18 W/m K, respectively. The material constants of the P–V–T equation for PS are listed in Table I.

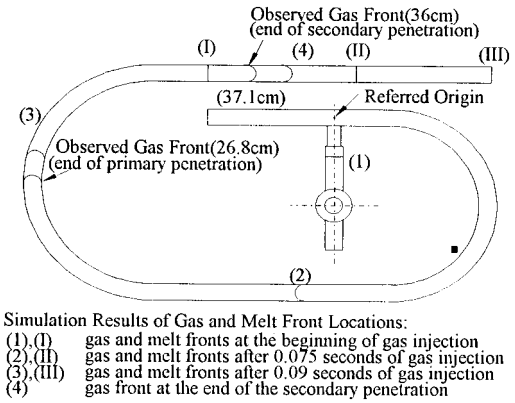

Figure 9 Comparison of the simulated and experimental observations of the gas-front locations during the primary and secondary gas penetration.

RESULTS AND DISCUSSION

Case of Spiral Part (One-dimensional Flow)

The first test example is a spiral tube. The spiral tube was gas-assisted injection-molded and the distribution of skin melt thickness was carefully measured along the gas-penetration path.[11] The skin melt thickness friction measured from experiments was about 0.36. Using this measured ratio, the gas-front advancement at different primary

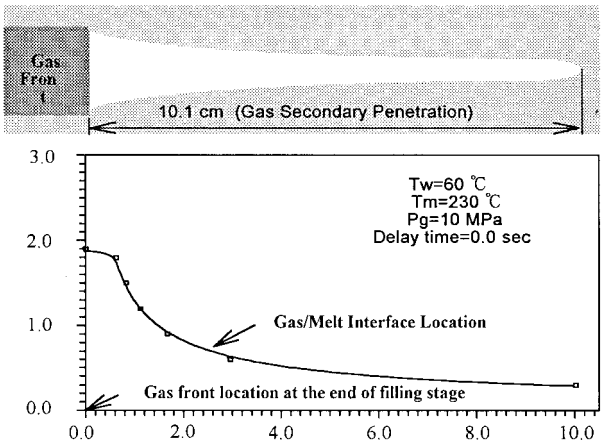

Figure 10 Simulated result of the skin melt distribution along the gas penetration direction during secondary penetration period.

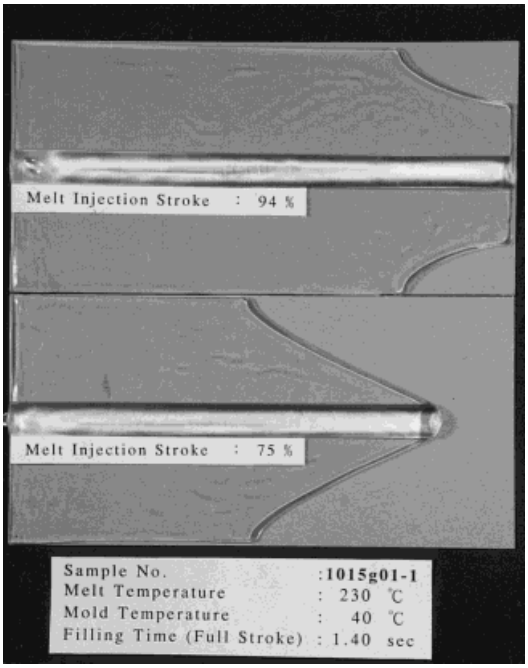

Figure 11 Melt-front locations after 1.05 and 1.31 s of melt injection for the plate part with a semicircular gas channel.

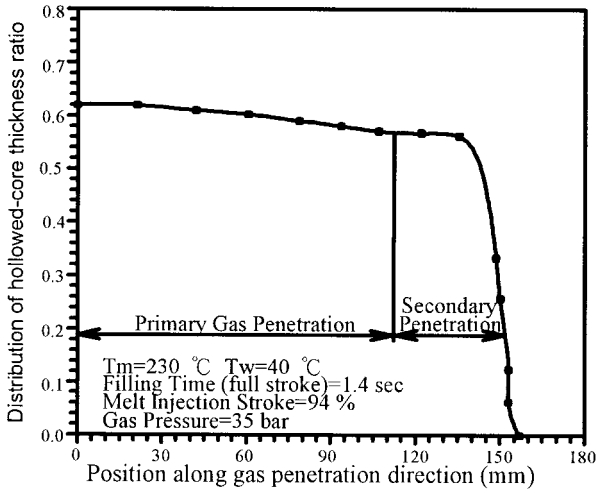

Figure 13 Distribution of thickness ratio for hollowed core along gas channel. The associated view of cored-out cross section by gas is also depicted.

gas-penetration stages was simulated. The secondary gas penetration during the postfilling phase was also simulated using the pressure, the gapwise temperature profile, and the P–V–T equation of state. An experimental observation of the gas front location (26.8 cm) at the end of filling process is indicated in Figure 8.

The simulated result of the primary gas-penetration length (27.2 cm) shows reasonably good consistency with experimental observation. The final gas front was located at a distance of 36 cm

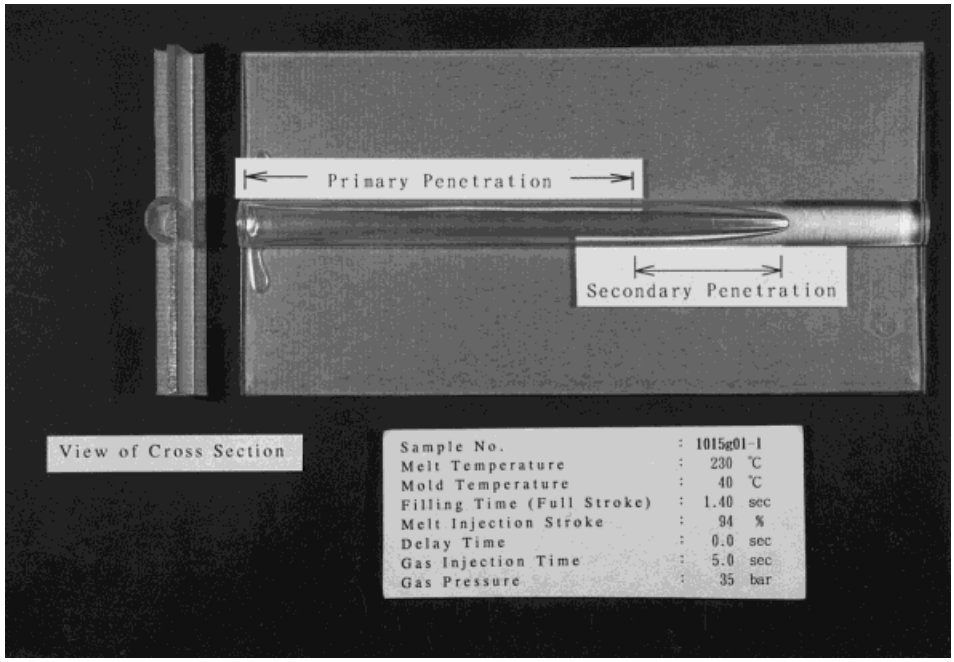

Figure 12 Gas-assisted injection-molded plate showing both the primary and secondary gas penetration.

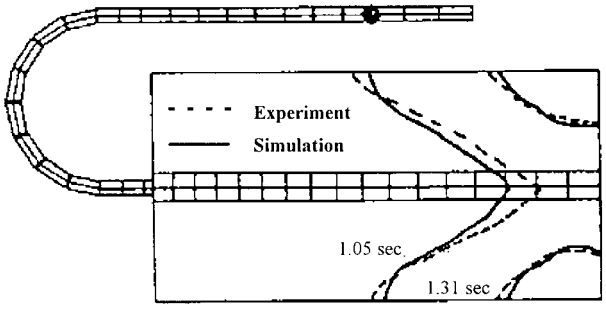

Figure 14 Comparison of simulated results and experimental observations on the melt-front locations during and at the end of melt-injection process.

away from the referred origin. The simulated gas-penetration length for the secondary phase is 10.1 cm, corresponding to a final gas-front location at 37.3 cm away from the referred origin. The consistency between the predicted value and the experimental result, as shown in Figure 9, is also very good. The hollowed core resulting from secondary gas penetration also shows a similar geometry as compared with the actual case (Fig. 10).

Case of a Thin Plate with a Gas channel of Semicircular Cross Section: Mixed Characteristics of One-dimensional and Two-dimensional Flow

This part of the geometry represents mixed 1-D and 2-D flow characteristics for both the melt and gas. Short shot experiments corresponding to a 73.7 and 94% of the full melt-injection stroke are shown in Figure 11. From these short shot experiments, the final melt-front locations prior to gas injection can be identified. Based on the formula given in Figure 5, the calculated equivalent diameter D_{eq} for the semicircular gas channel was 12.18 mm and the value of the shape factor was 0.928. The analyzed conditions were 0.9 s filling time for full shot and gas injection at a 94% melt-injection stroke (corresponding to 1.31 s of melt injection). The injected gas pressure was 130 bar. The gas injection-molded part can be seen in Figure 12. The distribution of the skin melt thickness along the gas channel and the corresponding view of a cored-out cross section is depicted in Figure 13. From the area of the cored-out section and the total area of the cross section (or the area enclosed by the tube of equivalent diameter), the estimated ratio for the hollowed core thickness was about 0.60. From the variation of the hollowed core thickness ratio, the estimated length for the primary gas penetration is 11.3 mm (within an error range of about 5%), corresponding to the gas-front location shown in Figure 12. The averaged melt shrinkage value calculated from the P–V–T equation of state is about 6%, corresponding to a 44 mm length for the secondary gas penetration. The estimated length for the secondary phase of the gas penetration is consistent with that found from the variation profile of the hollowed core thickness ratio as indicated in Figure 13. A comparison of the simulated and observed locations of the melt front is depicted in Figure 14. Simulated results for both gas- and melt-front advancements after 0.06 s of gas injection and at the end of the filling stage are shown in Figure 15(a) and (b), respectively. The predicted value for primary gas penetration is 10.6 cm, in good consistence with the observed one (11.3 cm). The calculated secondary gas penetration (with a length of 45 mm) is shown in Figure 15(c). Again, the predicted results for both gas-front locations at the end of the primary and secondary penetrations are also in good coincidence with observations.

CONCLUSIONS

Numerical simulations and experimental studies concerning gas and melt flow during the filling and the postfilling stages in gas-assisted injection molding of a spiral tube and a thin plate with a gas-channel design were conducted. Distributions of the skin melt thickness along the gas-flow direction were measured. A numerical algorithm based on the control-volume/finite-element method combined with dual-filling parameter technique suitable for two flow-front tracing schemes was developed to simulate gas- and melt-front advancement and the associated primary gas penetrations during the melt-filling and gas-assisted filling processes. Melt and gas flow in the gas channel of a semicircular cross section were approximated by a flow model which superimposes a circular pipe of equivalent diameter on the thin plate. An isotropic melt-shrinkage-induced flow model was implemented to predict secondary gas penetration and melt flow in the postfilling stage. Simulated results are also compared with experimental observations. All the verifications of simulations

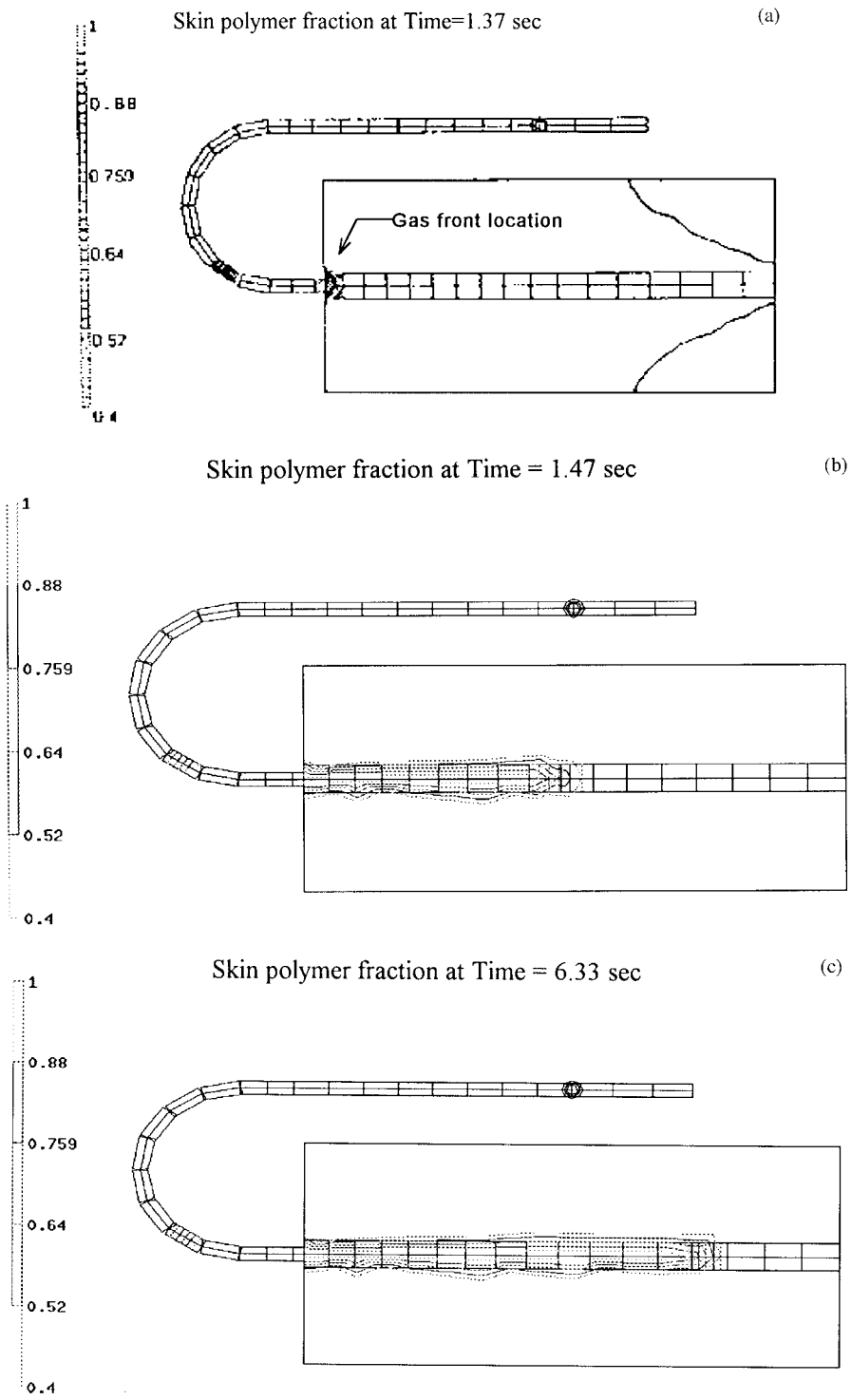

Figure 15 (a) Simulated result of gas-front location after 0.406 s of gas injection. (b) Simulated result of gas-front location at the end of primary gas penetration. (c) Simulated result of gas-front location at the end of secondary gas penetration.

in 1-D and mixed 1-D and 2-D conditions by the experiments are confirmed. Although the effects of processing conditions on the skin layer ratio remain to be investigated to establish a general empirical formula so that the skin layer ratio does not have to be known as priori, the current

numerical scheme provides reasonably good results in the prediction of gas penetration for both the primary and the secondary phases in the gas-assisted injection-molding process.

This work was supported by National Science Council under NSC grant 84-2622-E033-002R.

REFERENCES

1. K. C. Rush, *Plast. Eng.,* **July,** 35–38 (1989).
2. S. Shah, *SPE Tech. Pap.,* **37,** 1494–1506 (1991).
3. L. S. Turng, *SPE Tech. Pap.,* **38,** 452–456 (1992).
4. S. Shah and D. Hlavaty, *SPE Tech. Pap.,* **37,** 1479–1493 (1991).
5. V. W. Wang, C. A. Hieber, and K. K. Wang, *J. Polym. Eng.,* **7,** 21–45 (1986).
6. A. Davidoff, S. C. Chen, and H. Bung, *SPE Tech. Pap.,* **36,** 393–396 (1990).
7. S. C. Chen and K. F. Hsu, *Num. Heat Transfer A,* **28,** 121–129 (1995).
8. S. C. Chen and K. F. Hsu, *Num. Heat Transfer A,* **28,** 503–515 (1995).
9. S. C. Chen, K. F. Hsu, and K. S. Hsu, *Int. J. Heat Mass Transfer,* **39,** 2957–2968 (1996).
10. A. Lanvers and W. Michaeli, *SPE Tech. Pap.,* **37,** 1796–1800 (1992).
11. S. C. Chen, K. S. Hsu, and J. S. Huang, *Ind. Eng. Chem. Res.,* **34,** 416–420 (1995).
12. S. C. Chen, M. C. Jeng, K. S. Hsu, and K. F. Hsu, *Study of Gas-assisted Injection Molding Process and Its Computer Integrated Manufacturing Technology,* Progress Report of NSC, (1994).
13. S. C. Chen, P. Pai, and C. Hsu, *Annu. Tech. Pap. SPE,* **34,** 250–254 (1988).
14. K. H. Huebner and E. A. Thornton, *The Finite Element Method for Engineers,* Wiley, New York, 1982, Chaps. 4 and 5.
15. H. H. Chiang, C. A. Hieber, and K. K. Wang, *Polym. Eng. Sci.,* **31,** 116–124 (1991).